Journal of Solid State Chemistry 181 (2008) 1347–1353

Contents lists available at ScienceDirect

Journal of Solid State Chemistry

journal homepage: www.elsevier.com/locate/jssc

Two isotypic diphosphates $LiM_2H_3(P_2O_7)_2$ (M = Ni, Co) containing ferromagnetic zigzag MO_6 chains

Tao Yang, Sihai Yang, Fuhui Liao, Jianhua Lin *

Beijing National Laboratory for Molecular Sciences, State Key Laboratory of Rare Earth Materials Chemistry and Applications, College of Chemistry and Molecular Engineering, Peking University, Beijing 100871, PR China

ARTICLE INFO

Article history:
Received 4 December 2007
Received in revised form
8 March 2008
Accepted 10 March 2008
Available online 18 March 2008

Keywords:
Nickel
Cobalt
Phosphate
Ferromagnetic
Metamagnetic

ABSTRACT

Two new isotypic phosphates $LiNi_2H_3(P_2O_7)_2$ (**1**) and $LiCo_2H_3(P_2O_7)_2$ (**2**) have been hydrothermally synthesized and structurally characterized by the single-crystal X-ray diffraction technique. They crystallize in the monoclinic space group $C2/c$ with the lattice: $a = 10.925(2)$ Å, $b = 12.774(3)$ Å, $c = 8.8833(18)$ Å, $\beta = 123.20(3)^\circ$ for **1** and $a = 10.999(2)$ Å, $b = 12.863(3)$ Å, $c = 8.9419(18)$ Å, $\beta = 123.00(3)^\circ$ for **2**. The transition metal atoms are octahedrally coordinated, whereas the lithium and phosphorus atoms are all tetrahedrally coordinated. As the lithium-induced derivatives of $MH_2P_2O_7$ (M = Ni, Co), **1** and **2** possess the same structure with $MH_2P_2O_7$ in terms of topology, comprising the MO_6 zigzag chains and P_2O_7 as the interchain groups. The magnetisms of **1** and **2** could be interpreted by adopting a quasi-one-dimensional (1D) zigzag chain model as that in their parent compounds: both **1** and **2** have ferromagnetic (FM) NiO_6/CoO_6 chains; **1** shows a FM cluster glass behavior at low temperatures, which is originated from the possible antiferromagnetic (AFM) next-nearest-neighbour intrachain interactions; **2** shows a AFM ordering at $T_N = 2.6$ K and a metamagnetic transition at $H_C = 4.2$ kOe at 1.8 K.

© 2008 Elsevier Inc. All rights reserved.

1. Introduction

The low-dimensional magnetism is well known to be of great interest to both physicists and chemists, because it is propitious to understand the superconductivity of cuprates [1]. Recently, a number of transition metal phosphates have been proved to exhibit outstanding one-dimensional (1D) magnetic characteristics, including antiferromagnetic (AFM), ferrimagnetic, and ferromagnetic (FM) chains [2–12]. For example, $M_2Cu(PO_4)_2$ (M = Ba, Sr) [4,5] and $ACuP_2O_7$ (A = Sr, Pb, Ba) [6,7] behave as typical 1D uniform $S = 1/2$ Heisenberg AFM chains, $ACu_2(PO_4)_2$ (A = Sr, Pb) shows linear AFM interactions and has a spin gap above the spin-singlet ground state, which leads to a 1/2 magnetization plateau observed between 50 and 63 T at 1.3 K for $SrCu_2(PO_4)_2$ [8,9]. Ferrimagnetic chains have been observed in a series of phosphates $AM_3P_4O_{14}$ (A = Sr, Ba; M = Ni, Co, Mn) [10,11], in which the edge-sharing MO_6 zigzag chains all adopt the same AFM–AFM–FM trimerized model, interestingly, only the Mn analogs show 1/3 quantum magnetization plateaus. In addition, FM chains are reported in $MH_2P_2O_7$ (M = Ni, Co) [12], which consists of edge-sharing zigzag MO_6 chains and P_2O_7 as inter-groups; these FM MO_6 chains are antiferromagnetically coupled in $MH_2P_2O_7$ and thus, a typical metamagnetism has been observed.

In this work, $LiNi_2H_3(P_2O_7)_2$ (**1**) and $LiCo_2H_3(P_2O_7)_2$ (**2**), as two lithium-induced derivatives of $MH_2P_2O_7$, have been synthesized by hydrothermal methods and analyzed by single-crystal X-ray diffraction; **1** and **2** are identical with $MH_2P_2O_7$ in terms of topology and just differ in crystal symmetry and therefore, they can also be viewed as quasi-1D magnets. The magnetic measurements have showed that both **1** and **2** possess FM NiO_6/CoO_6 chains; the interchain interaction is FM in **1** but AFM in **2**.

2. Experimental section

2.1. Syntheses

All reagents were of analytical grade and were used as obtained from commercial sources without further purification. $LiM_2H_3(P_2O_7)_2$ (M = Ni, Co) were synthesized under hydrothermal conditions at 200 °C. Typically, we charged a powder mixture of 1.5 mmol $LiNO_3$ and 3 mmol $M(CH_3COO)_2 \cdot 4H_2O$ (M = Ni, Co) into a 50 mL Teflon reactor, then added in 3 mL concentrated H_3PO_4 and sealed the reactor into a stainless-steel container. After they were heated at 200 °C for 5 days, the solid products were extensively washed by hot water (80 °C). The obtained

* Corresponding author. Fax: +86 10 62751708.
E-mail address: jhlin@pku.edu.cn (J.H. Lin).

0022-4596/$ - see front matter © 2008 Elsevier Inc. All rights reserved.
doi:10.1016/j.jssc.2008.03.006

Fig. 1. Morphology of $LiCo_2H_3(P_2O_7)_2$ single crystals.

single-crystals are block-like, purple for **1** and green for **2**. A photo of crystals is shown in Fig. 1. The yields of the products, estimated on the basis of the transition metal salts, are about 80%. Other transition metal resources, such as bivalent metal chlorides or nitrates, can also yield the same products.

2.2. Analyses

Representatively, a crystal of $LiCo_2H_3(P_2O_7)_2$ with approximate dimensions $0.2 \times 0.25 \times 0.3\ mm^3$ was selected and used for single-crystal diffraction data collection at room temperature on a Rigaku AFC6S diffractometer with graphite-monochromated Mo $K\alpha$ radiation ($\lambda = 0.71073$ Å) by using the ω–2θ scan method. The structure was solved by direct methods and refined on F^2 with full-matrix least-squares methods using SHELXS-97 and SHELXL-97 programs [13]. Cobalt, phosphorus and part of the oxygen atoms of the framework were directly located. Lithium and the other atoms were found by difference Fourier maps. For the final refinement, the hydrogen atoms were placed in geometrically ideal positions and refined in the riding model. The same treatment was performed on a single-crystal of $LiNi_2H_3(P_2O_7)_2$. The detailed crystallographic information is given in Table 1 [14].

Powder magnetic susceptibilities as a function of temperature were performed on a Quantum Design MPMS XL-7 SQUID system at an applied field of 100 Oe. Crystals of $LiM_2H_3(P_2O_7)_2$ (M = Ni, Co) were ground and placed in a gelatin capsule fastened in a plastic straw for immersion into the SQUID system. The isothermal magnetization curves were measured at 1.8 K up to 7 T. The ac magnetic susceptibilities were measured at a 3 Oe oscillating field and frequency range of 1–997 Hz. Chemical analyses were carried out using inductively coupled plasma (ICP) methods on an ESCALAB2000 analyzer. The measured ratios, Li:Co:P ≈ 1:1.90:3.92 and Li:Ni:P ≈ 1:1.92:3.86, agree well with the proposed formula. The thermogravimetric–differential scanning calorimetric–mass spectrometric (TG–DSC–MS) measurements were carried out on a NETZSCH STA449C instrument at a heating rate of 10 °C/min from 40 to 800 °C under an air atmosphere. Powder X-ray diffraction data were collected at room temperature on a Rigaku D/Max-2000 diffractometer (Cu $K\alpha$, $\lambda = 1.5406$ Å, 40 kV and 100 mA, graphite monochromator, scintillator detector, step scan 0.02°/3 s).

Table 1
The crystallographic parameters and refinement results of $LiM_2H_3(P_2O_7)_2$ (M = Ni, Co)

Formula	$LiNi_2H_3(P_2O_7)_2$	$LiCo_2H_3(P_2O_7)_2$
CSD-number	417375	417374
Formula mass	475.26	475.7
Radiation λ (Å)	0.71073	0.71073
Crystal size (mm)	$0.2 \times 0.25 \times 0.3$	$0.2 \times 0.25 \times 0.3$
Morphology	Block, green	Block, purple
Space group	$C2/c$	$C2/c$
a (Å)	10.925(2)	10.999(2)
b (Å)	12.774(3)	12.863(3)
c (Å)	8.8833(18)	8.9419(18)
β (deg)	123.20(3)	123.00(3)
V (Å^3)	1037.4(4)	1060.9(4)
Z	4	4
ρ_{calcd} (g cm^{-3})	3.043	2.978
μ(Mo $K\alpha$) (mm^{-1})	4.334	3.815
Reflections collected	1018	1041
Independent reflections	970	991
$I > 2\sigma(I)$	857	952
R_{int}	0.0630	0.0107
θ range (degree)	2.74–25.48	2.72–25.48
GOF	1.094	1.063
R_1/wR_2[a] ($I > 2\sigma(I)$)	0.0281/0.0740	0.0353/0.1224
R_1/wR_2 (all data)	0.0348/0.0772	0.0366/0.1237

[a] $R_1 = \Sigma(||F_o|-|F_c||)/\Sigma|F_o|$; $wR_2 = \Sigma[w(F_o^2-F_c^2)^2/\Sigma[w(F_o^2)^2]^{1/2}$, where $w = 1/[\sigma^2(F_o^2)+(0.0700P)^2+7.26P]$ with $P = \max(F_o^2+2F_c^2)/3$.

3. Results and discussion

3.1. Structure description

The title compounds are lithium-induced derivatives of two reported diphosphates $MH_2P_2O_7$ (M = Ni, Co) [12]. It is interesting that, with the incorporation of lithium ions, the structural symmetry increases from $P2_1/c$ in $MH_2P_2O_7$ to $C2/c$ in $LiM_2H_3(P_2O_7)_2$ (M = Ni, Co). Here we describe the structure of $LiCo_2H_3(P_2O_7)_2$ as being representative. From the single-crystal X-ray diffraction analysis, there are in total 14 crystallographic independent atoms in an asymmetric unit: Co1 and Li reside in the two-fold axis (4*e* site) and Co2 resides in the inverse center (4*c* site); the rest of the atoms, including 2P, 7O and 2H are all located in general positions. One of the hydrogen atoms (H6) is half occupied, according to the charge balance. As sketched in Fig. 2, the cobalt atoms are both octahedrally coordinated, whereas the lithium and phosphorus atoms are all tetrahedrally coordinated. The selected bonds and torsion angles are given in Table 2, which are all regular as that in other related compounds. Every CoO_6 octahedron shares edges with adjacent two CoO_6, forming infinite zigzag chains along the *a*-axis; while, each two PO_4 tetrahedra were dimerized into a P_2O_7 group by sharing the common O3; the CoO_6 chains and P_2O_7 groups are interconnected to a three-dimensinal framework (see Fig. 3). The nearest intrachain M–M distances are about 3.12 Å in **1** and 3.16 Å in **2** via double oxo-bridges; while the nearest interchain M–M distance is about 5.05 Å in **1** and 5.06 Å in **2** via an O–P–O linkage.

The bond valence sums (BVS) calculation indicates that all the transition metal ions are normally divalent (BVS = 1.952 (Ni1), 2.012 (Ni2) for **1**, 1.980 (Co1), 2.054 (Co2) for **2**) [15]. The thermal stabilities of as-synthesized $LiM_2H_3(P_2O_7)_2$ (M = Ni, Co) have been investigated by TG–DSC–MS measurements (see Fig. 4). Both of them show a single and steep mass loss (exptl. ~6.0 wt%; calcd. 5.7 wt%) at about 550 °C for **1** and 450 °C for **2**, respectively, corresponding to the dehydration of the hydroxyl groups. Such a dehydration process can also be detected by the prominent endothermic peak at DSC curves and significant peaks at mass spectra in the same temperature region. For a better

understanding of the dehydration, we annealed the $LiM_2H_3(P_2O_7)_2$ at different temperatures (25, 200, 300, 400, 500, 600, 700, and 750 °C) for over 10 h, and after every heating treatment, we cooled the sample and collected the powder X-ray diffraction data as shown in Fig. 5. Before the dehydration, the diffraction patterns remain unchanged, reflecting that the framework remains intact; after that, the diffraction patterns become relatively complicated, which indicates that **1** (and **2**) decompose into several phases. In principle, according to the stoichiometric amount of the system, Li:*M*:P = 1:2:4 (*M* = Ni, Co), the decomposed products could be confirmed by analyzing the Li–*M*–P–O quasi-ternary phase diagrams. According to the Rietveld refinements on the diffraction data of the 700 and 750 °C annealed samples using Topas [16], we found four known phosphates, $LiM_2P_3O_{12}$, $M_2P_4O_{12}$, $Li_4P_2O_7$, and a trace of $M_2P_2O_7$ [17–21]; it is apparent that the system has not yet achieved the thermodynamic equilibrium after 10 h annealing. As an intermediate state, the diffraction pattern of the 500 °C annealed sample seems quite different with both the low and high temperature ones and it is difficult to verify the decomposed phases; there probably contains an unknown phase, which needs further investigations.

3.2. Magnetism

Fig. 6 shows the connectivity of the Ni backbone in **1**, which is in fact topologically the same with that in $NiH_2P_2O_7$: the nearest-neighbour (NN) and next-nearest-neighbour (NNN) intrachain distances are ~3.12 Å between Ni1 and Ni2, and ~4.80 Å between Ni2 and Ni2 through an O–P–O linkage, respectively; the nearest interchain distance is ~5.05 Å between Ni1 and Ni1 atoms also through an O–P–O linkage. $MH_2P_2O_7$ (*M* = Ni, Co) have been reported as quasi-1D metamagnets, where the intrachain and interchain interactions are FM and AFM, respectively. Thus, it is understandable to interpret the magnetism of the title compounds also as quasi-1D systems, whereas the specific interactions could be different with those in $MH_2P_2O_7$ (*M* = Ni, Co).

With a polycrystalline sample, the temperature-dependent magnetic susceptibility of **1** was measured in the range of 2–300 K at 100 Oe both under zero field cooling (ZFC) and field cooling (FC) conditions (see Fig. 7). The reciprocal susceptibility χ^{-1} (T) above 25 K follows the Curie–Weiss law quite well with a result of $\theta = 14.1$ K, $C = 1.22\ cm^3\ K\ mol^{-1}$ as shown in the left inset of Fig. 7. The Curie constant is typical for an isolated Ni^{2+} (d^8, $S = 1$) system

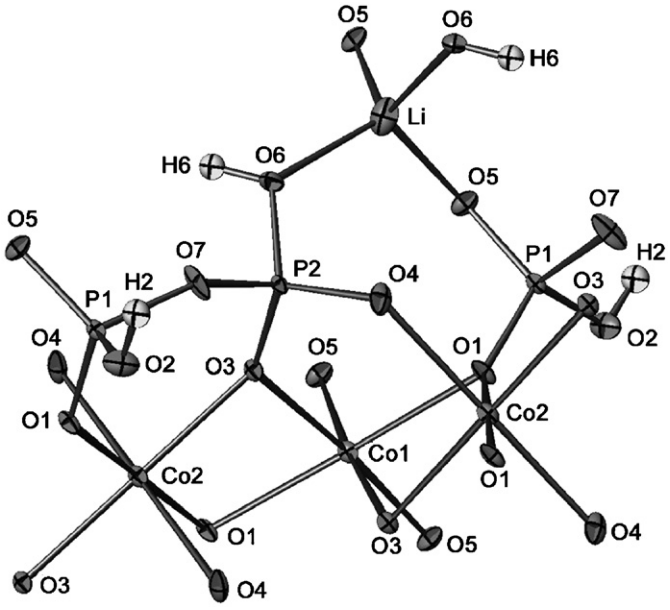

Fig. 2. A fragment of $LiCo_2H_3(P_2O_7)_2$ shows the coordination environments of cobalt, phosphorus, and lithium.

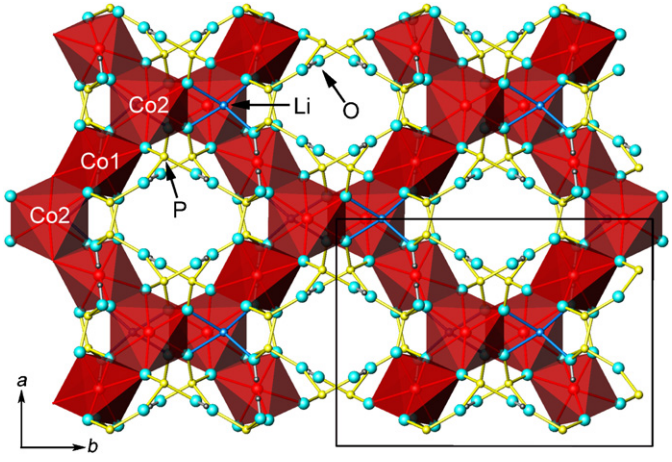

Fig. 3. A view along the {001} direction shows the zigzag CoO_6 chains running along the *a*-axis.

Table 2
Selected bond distances (Å) and torsion angles (deg) for $LiM_2H_3(P_2O_7)_2$ (*M* = Ni, Co)

Bond	1	2	Angle	1	2	Angle	1	2
*M*1–O5(×2)	2.030(3)	2.054(3)	O5–*M*1–O5	81.31(15)	81.00(15)	O5–Li–O5	84.0(5)	84.5(4)
*M*1–O3(×2)	2.076(3)	2.101(3)	O5–*M*1–O3	98.74(11)	98.83(10)			
*M*1–O1(×2)	2.107(3)	2.159(3)	O3–*M*1–O3	81.85(15)	81.75(14)	O5–P1–O1	113.15(16)	113.22(16)
*M*2–O1(×2)	2.033(3)	2.051(3)	O5–*M*1–O1	90.13(11)	89.30(11)	O5–P1–O2	114.52(16)	114.47(16)
*M*2–O3(×2)	2.044(3)	2.092(3)	O5–*M*1–O1	95.72(11)	96.76(10)	O1–P1–O2	108.36(16)	108.04(15)
*M*2–O4(×2)	2.102(3)	2.127(3)	O3–*M*1–O1	78.28(10)	78.43(10)	O5–P1–O7	106.30(17)	106.53(16)
P1–O5	1.498(3)	1.506(3)				O1–P1–O7	109.08(16)	109.21(15)
P1–O1	1.516(3	1.518(3)	O3–*M*1–O1	95.83(11)	95.49(10)	O2–P1–O7	104.99(17)	104.95(17)
P1–O2	1.538(3)	1.536(3)	O1–*M*2–O3	99.28(10)	98.89(10)			
P1–O7	1.583(3)	1.584(3)	O1–*M*2–O3	80.72(10)	81.11(10)	O4–P2–O3	112.81(16)	112.64(16)
P2–O4	1.508(3)	1.511(3)	O1–*M*2–O4	92.18(11)	91.82(11)	O4–P2–O6	111.66(16)	111.54(16)
P2–O3	1.520(3)	1.517(3)	O1–*M*2–O4	87.82(11)	88.18(11)	O3–P2–O6	112.11(16)	112.15(15)
P2–O6	1.532(3)	1.534(3)	O3–*M*2–O4	97.63(11)	97.62(11)	O4–P2–O7	107.41(17)	107.21(17)
P2–O7	1.589(3)	1.589(3)	O3–*M*2–O4	82.37(11)	82.38(11)	O3–P2–O7	107.62(16)	107.88(15)
Li–O5(×2)	1.976(9)	1.984(8)				O6–P2–O7	104.69(17)	104.93(17)
Li–O6(×2)	1.978(8)	1.979(7)	O6–Li–O6	101.1(5)	102.5(5)			
H6–O6	0.819(3)	0.821(3)	O6–Li–O5	119.78(13)	116.69(12)			
H2–O2	0.819(3)	0.821(3)	O6–Li–O5	116.56(13)	118.48(12)			

and the positive value of θ suggests predominant FM interactions between nickel atoms. In the low-temperature region, the susceptibility shows a very sharp increase, from 0.34 $cm^3 mol^{-1}$ at 12 K to 11.7 $cm^3 mol^{-1}$ at 5.4 K, which points to the FM nature of the sample again; the FC–ZFC curves diverge at about 5.4 K, suggesting a possible magnetic ordering with a spontaneous magnetism. The ordering temperature could be estimated from the differential of the χT curve, which shows a pronounced and negative peak at 5.6 K (see the right inset of Fig. 7). The relatively low T_C compared to the θ ($\theta/T_C = 2.5$) also confirms our former assumption about the quasi-low dimensionality of the Ni system.

In addition, the ZFC curve exhibits a decrease with reducing temperature, indicating the lack of a true long-range ordering. This is a typical characteristic of a spin glass (SG) or cluster glass (CG) [22–24]. In view of the magnetic structure, a SG usually exhibits frozen magnetic moments below the freezing temperature, and a lack of periodic long-range magnetic order, whereas a CG can be considered to be a modified version of the SG system and a set of clusters, formed due to short-range ordering at temperatures near the Curie-like temperature T_C [25]. The ac susceptibilities for **1** at different frequencies (see Fig. 8) show a slightly frequency-dependent feature as expected for a glassy magnet. It is believed that the peaks at ~5.5 K in χ' and ~4.5 K in χ'' are related to the Curie-like ordering, and the shoulder-peaks at

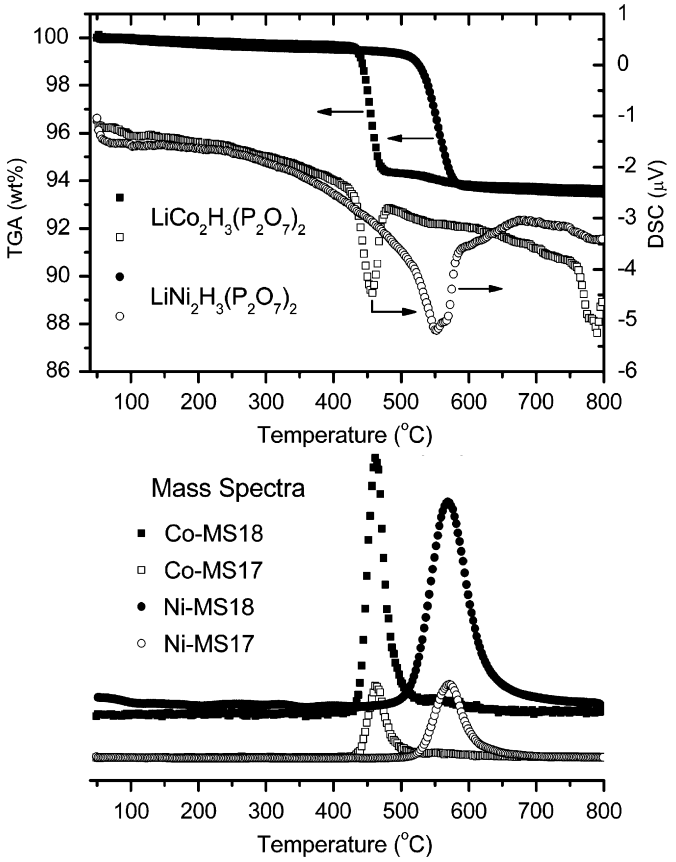

Fig. 4. TG–DSC–MS curves of the as-synthesized Li$M_2H_3(P_2O_7)_2$ (M = Ni, Co).

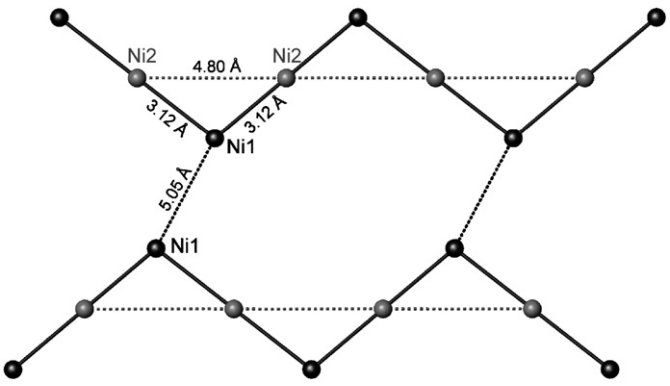

Fig. 6. Topological connectivity of the Ni backbone in $LiNi_2H_3(P_2O_7)_2$.

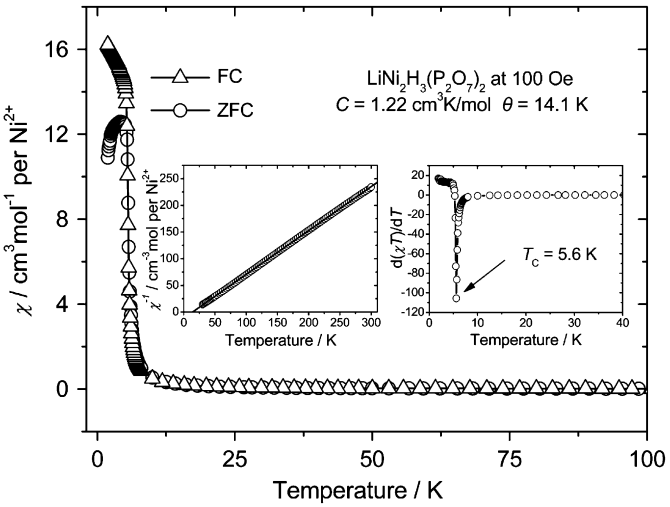

Fig. 7. Temperature-dependent dc susceptibilities for **1** at 100 Oe under both ZFC and FC conditions. The left and right insets are the Curie–Weiss fit of the reciprocal susceptibility χ^{-1} and the d(χT)/dT curve, respectively.

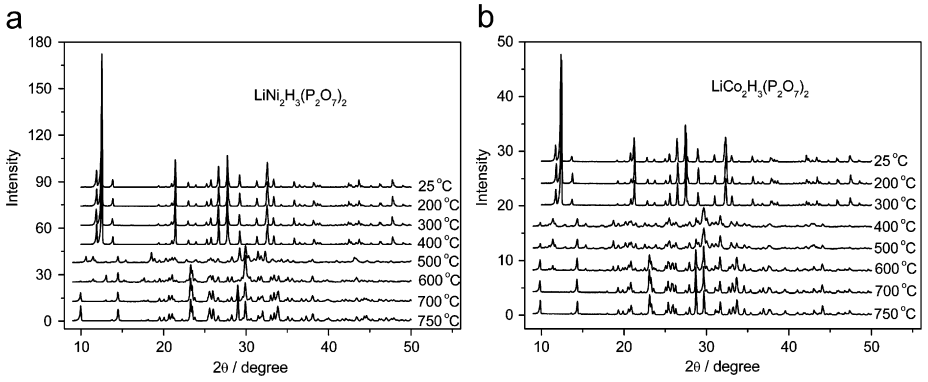

Fig. 5. Powder X-ray diffraction patterns collected on the annealed Li$M_2H_3(P_2O_7)_2$ (M = Ni, Co) samples at different temperatures.

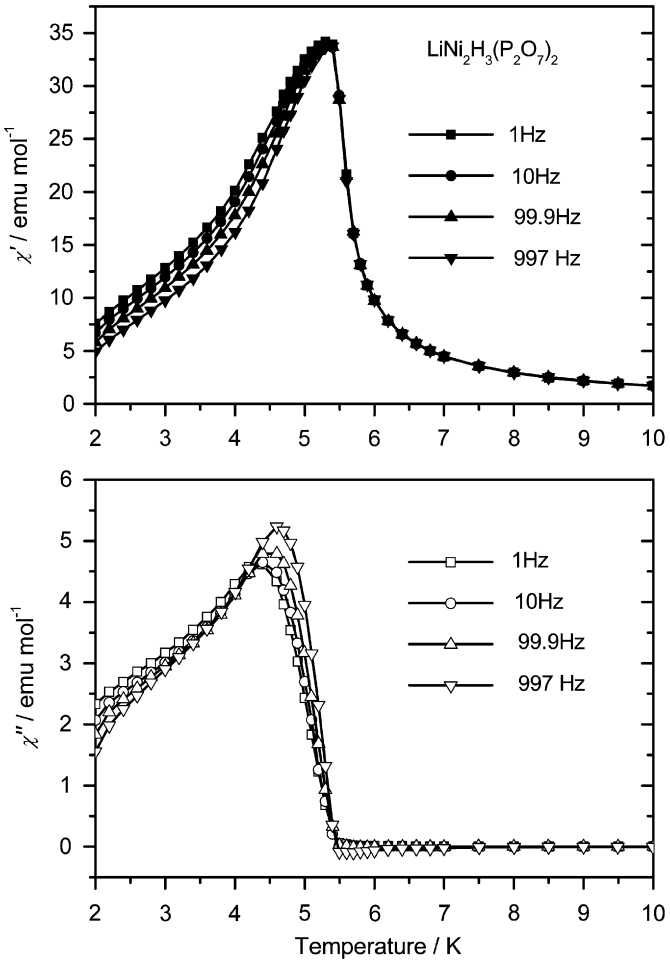

Fig. 8. Temperature-dependent ac susceptibilities (χ', in-phase signals; χ'', out-of-phase signals) for **1** at frequencies of 1 (■/□), 10 (●/○), 99.9 (▲/△), and 997 Hz (▼/▽).

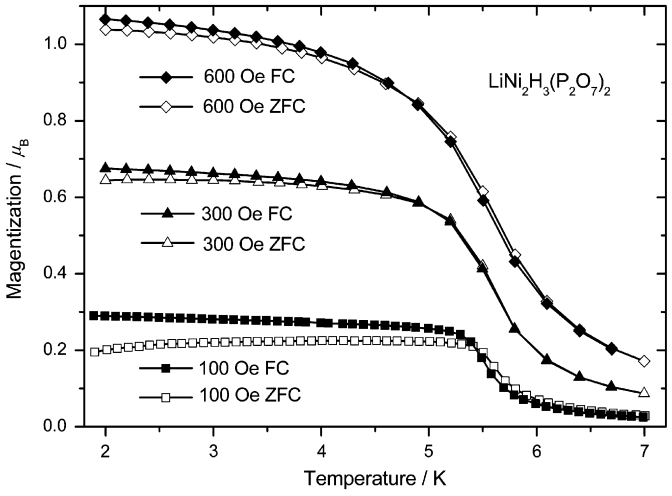

Fig. 9. ZFC–FC curves for **1** under different external fields (100, 300, and 600 Oe).

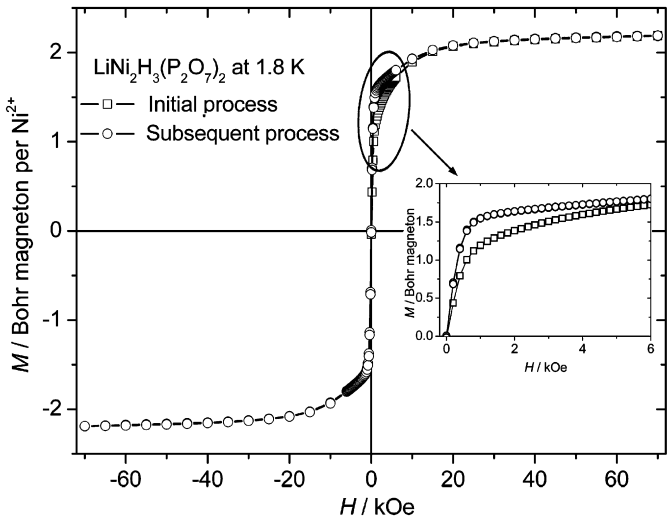

Fig. 10. Field dependence of the magnetization plot for **1** at 1.8 K. The inset is the enlargement in the low field region.

~3 K in χ' and ~2.5 K in χ'' may correspond to the freezing point of CG.

It is commonly accepted that the glassy behavior of SG or CG is originated from site disordering or the competitions between magnetic couplings. The former one seems unreasonable because **1** is a homometallic chain compound with full occupancies of metal sites; and therefore, we prefer to contribute this glassy behavior to the latter reason. It is known that the zigzag chain model with the consideration of the NNN interactions actually could be a 1D frustrated spin system under certain conditions. For example, the spins of Ni1 and Ni2 within a single chain should have the same orientation in an ordered state because of the strong FM NN interaction; if the NNN interaction of Ni2–O–P–O–Ni2 was AFM, the spin orientation of Ni2 would be somewhat frustrated. Because of the positive value of θ (14.1 K), which is an algebraic sum of all the magnetic exchange interactions, the AFM NNN intrachain interaction, even if it existed, should be small and the frustration effect should also be quite weak; this hypothesis is reinforced by the ZFC–FC curves measured under different external fields. As shown in Fig. 9, the ZFC signals under 300 and 600 Oe monotonously increase from 7 to 2 K, indicating that 300 Oe is strong enough to compromise the possible AFM NNN interaction and eliminate the glassy behavior.

Fig. 10 shows the isothermal magnetization curve of **1** at 1.8 K. It shows a very quick saturation at ~2.18μ_B, slightly higher than the theoretical value (2μ_B) expected from a spin-only system, which is coincident with the strong FM interactions between Ni atoms. Note that there is an unusual irreversibility between the initial magnetization and the subsequent demagnetization/re-magnetization processes (see the inset of Fig. 10). At such a low temperature (1.8 K), the CG tends to be frozen at low fields and after a magnetization/demagnetization cycle, the spins should at least partially remain the high filed magnetized arrangement and show some sort of memory effect. This is the possible reason for the unusual irreversibility in the isothermal magnetization curve. **1** is a typical soft ferromagnet and has no magnetic remanence or coercive field, which is again an implication of the very weak interchain magnetic interactions (Ni1–O–P–O–Ni1).

As shown in Fig. 11a, the ZFC and FC curves of **2** at 100 Oe show no noticeable difference in the whole measured range. The high-temperature data fit the Curie–Weiss law with $C = 3.28$ $cm^3\,K\,mol^{-1}$, which is typical for Co^{2+} ions ($S = 3/2$) [26,27]. At first glance, because of the negative Weiss constant θ (−14.8 K), the comparatively small value of molar susceptibility of **2** (less than 1/10 of **1** at low temperature) and the maximum at ~2.8 K in χ, one may conclude that **2** is a conventional antiferromagnet with a long-range ordering temperature $T_N \approx 2.6$ K (see the inset of Fig. 11b). However, an abnormal upturn from 20 to 5 K in χT vs. T (see Fig. 11b) suggests a FM component. Additionally,

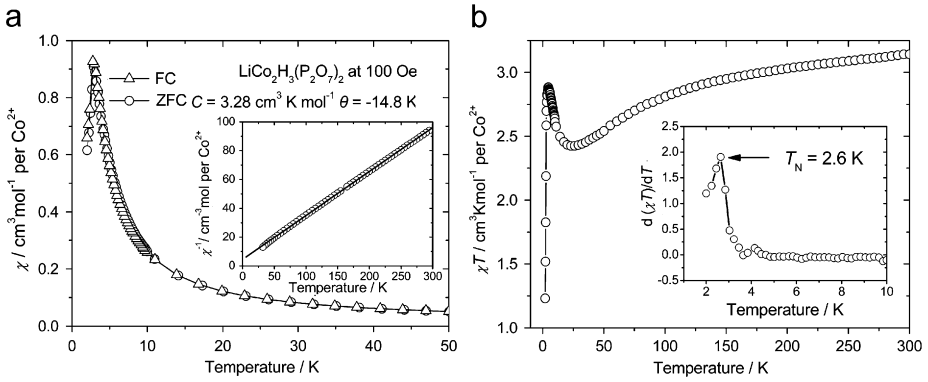

Fig. 11. (a) ZFC and FC curves for **2** at 100 Oe in the range of 2–50 K and the Curie–Weiss fitness of χ^{-1} above 30 K is the inset; (b) χT vs. T curve under the FC condition. The inset is the d(χT)/dT curve.

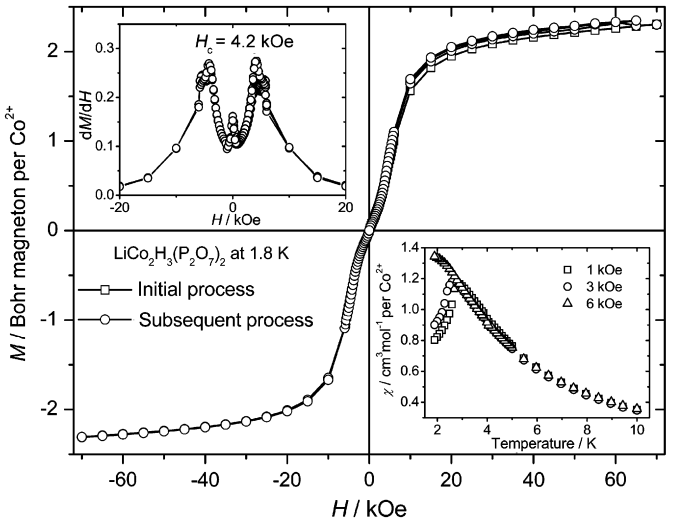

Fig. 12. Isothermal magnetization curve for **2** at 1.8 K. The left inset is the dM/dH curve and the right inset is the FC curves for **2** under different external fields.

the isothermal magnetization curve at 1.8 K shows a sharp increase in spite of a sigmoidal shape, which gives a positive proof that the main magnetic interactions between Co^{2+} ions are in fact FM. While, the negative θ is most likely the consequence of the single-ion behavior of Co^{2+}, which is common in other Co-compounds [12,28]. Compound **2** shows a similar metamagnetism with that of $CoH_2P_2O_7$: the critical field is ~4.2 kOe estimated from the dM/dH curve (see the left inset of Fig. 12); the metamagnetism is also confirmed by the FC curves under different magnetic fields (see the right inset of Fig. 12), where the maximum at 2.8 K is suppressed by the high field. Based on all the above observations, it is very likely that compound **2** comprises FM CoO_6 chains and these FM chains tend to be antiferromagnetically coupled to form an AFM ordering below 2.6 K at low fields. In contrast to the magnetic isotropy of Ni^{2+}, the large anisotropy of Co^{2+} is the possible origin of the AFM ordering of **2**.

4. Conclusions

In conclusion, two new diphosphates $LiM_2H_3(P_2O_7)_2$ (M = Ni, Co) have been obtained by hydrothermal synthesis and structurally characterized. As the lithium-induced derivatives of $MH_2P_2O_7$ (M = Ni, Co), **1** and **2** have the same structural topology with their parent compounds, comprising the MO_6 zigzag chains with P_2O_7 as the interchain groups. The magnetic investigation of **1** and **2** shows that although the magnetic ground states are different in **1** (FM) and **2** (AFM), importantly, both of them have the FM MO_6 chains and show quasi-1D characteristics. In fact, 1D ferromagnets are particularly interesting because their quantum effects are expected to be pronounced [29]. Here, the isotypic phosphates **1** and **2** are present as Heisenberg and Ising FM chain compounds, respectively. We hope this work will encourage the theoreticians to investigate this interesting zigzag FM chain model.

Acknowledgment

This work was supported by the Nature Science Foundation of China, under the Contract no. 20221101.

Appendix A. Supplementary material

Supplementary data associated with this article can be found in the online version at doi:10.1016/j.jssc.2008.03.006.

References

[1] P. Lemmens, G. Güntherodt, C. Gros, Phys. Rep. 375 (2003) 1.
[2] A.A. Belik, A. Matsuo, M. Azuma, K. Kindo, M. Takano, J. Solid State Chem. 178 (2005) 709–714.
[3] M. Matsuda, K. Kakurai, A.A. Belik, M. Azuma, M. Takano, M. Fujita, Phys. Rev. B 71 (2005) 144411.
[4] A.A. Belik, M. Azuma, M. Takano, J. Solid State Chem. 177 (2004) 883–888.
[5] A.A. Belik, S. Uji, T. Terashima, E. Takayama-Muromachi, J. Solid State Chem. 178 (2005) 3461–3463.
[6] A.A. Belik, M. Azuma, M. Takano, Inorg. Chem. 42 (2003) 8572–8578.
[7] A.A. Belik, M. Azuma, M. Takano, Inorg. Chem. 44 (2005) 7523–7529.
[8] A.A. Belik, M. Azuma, A. Matsuo, M.H. Whangbo, H.J. Koo, J. Kikuchi, T. Kaji, S. Okubo, H. Ohta, K. Kindo, M. Takano, Inorg. Chem. 44 (2005) 6632–6640.
[9] A.A. Belik, M. Azuma, A. Matsuo, T. Kaji, S. Okubo, H. Ohta, K. Kindo, M. Takano, Phys. Rev. B 73 (2006) 024429.
[10] M. Hase, H. Kitazawa, N. Tsujii, K. Ozawa, M. Kohno, G. Kido, Phys. Rev. B 74 (2006) 024430.
[11] T. Yang, Y. Zhang, S.H. Yang, G.B. Li, M. Xiong, F.H. Liao, J.H. Lin, Inorg. Chem. 47 (2008) 2562–2568.
[12] T. Yang, J. Ju, G.B. Li, S.H. Yang, J.L. Sun, F.H. Liao, J.H. Lin, J. Sasaki, N. Toyota, Inorg. Chem. 46 (2007) 2342–2344.
[13] G.M. Sheldrick, SHELXS97, Program for Crystal Structure Solution, University of Göttingen, Göttingen, Germany, 1997; G.M. Sheldrick, SHELXL97, Program for Crystal Structure Refinement, University of Göttingen, Göttingen, Germany, 1997.

[14] For further details of structure study, one may refer to the deposited data from the Fachinformationszentrum Karlsruhe, 76344 Eggenstein-Leopoldshafen, Germany (fax: (+49)7247-808-666; e-mail, crysdata@fiz-karlsruhe.de), on quoting the depository number CSD-417374 and CSD-417375.
[15] D. Brown, D. Altermatt, Acta Crystallogr. B 41 (1985) 244.
[16] TOPAS V2.1: General Profile and Structure Analysis Software for Powder Diffraction Data; Bruker AXS, Karlsruhe, Germany.
[17] F. Erragh, A. Boukhari, E.M. Holt, Acta Crystallogr. C 52 (1996) 1867–1869.
[18] K. Rissouli, K. Benkhouja, A. Sadel, M. Bettach, M. Zahir, M. Giorgi, M. Pierrot, M. Drillon, Euro. J. Solid State Inorg. Chem. 34 (1997) 221–230.
[19] A. Olbertz, D. Stachel, I. Svoboda, H. Fuess, Z. Kristallogr. New Cryst. Struct. 213 (1998) 241–242.
[20] O.V. Yakubovich, O.K. Melnikov, Kristallografiya 39 (1994) 815–820.
[21] R. Masse, J.C. Guitel, A. Durif, Mater. Res. Bull. 14 (1979) 337–341.
[22] J.W. Cai, C. Wang, B.G. Shen, J.G. Zhao, W.S. Zhan, Appl. Phys. Lett. 71 (1997) 1727–1729.
[23] D.S. Douglas, C. Leighton, Phys. Rev. B 70 (2004) 214414.
[24] S. Karmakar, S. Taran, B.K. Chaudhuri, H. Sakata, C.P. Sun, C.L. Huang, H.D. Yang, Phys. Rev. B 74 (2006) 104407.
[25] X.Y. Zhang, Y.J. Chen, Z.Y. Li, V. Vittoria, V.G. Harris, J. Phys.: Condens. Matter 19 (2007) 266211.
[26] F.E. Mabbs, D.J. Machin, Magnetism and Transition Metal Complexes, Chapman & Hall, London, 1973.
[27] B.N. Figgis, M.A. Hitchman, Ligand Field Theory and Its Applications, Wiley-VCH, New York, 2000.
[28] H.L. Sun, S. Gao, B.Q. Ma, G. Su, Inorg. Chem. 42 (2003) 5399–5404.
[29] A.A. Belik, M. Azuma, A. Matsuo, K. Kindo, M. Takano, Inorg. Chem. 44 (2005) 3762–3766 and the references cited therein.